# Chapter 11
# Mathematical Modelling of Piezoelectric Generators on the Base of the Kantorovich Method

Arkadiy N. Soloviev, Valerii A. Chebanenko, and Ivan A. Parinov

**Abstract** In this chapter, applied semi-analytical theories were constructed, allowing preliminary estimations of the output characteristics of piezoelectric generators (PEG) of various configurations. The developed theories are based on the Hamiltonian principle, extended to the theory of electroelasticity. In the first part of the work, within the framework of the Euler-Bernoulli hypotheses, a model for a cantilever PEG was developed. The main model's peculiarity is the consideration of the structural features of cantilever PEGs. In the second part, a model was developed for multilayer stacked PEGs, where the energy generation process was considered as forced oscillations of an electroelastic rod. Solutions for both cases were carried out using the Kantorovich method. The adequacy of the theories obtained in both cases was verified by comparison with finite-element calculations.

## 11.1 Introduction

In recent years, research of piezoelectric transducers that convict mechanical energy into electrical energy has been actively developed. This type of transducers is called piezoelectric generator (PEG). The basic information about PEG, as well as the

Arkadiy Nikolaevich Soloviev
Don State Technical University, Gagarin sq., 1 &
I. I. Vorovich Institute of Mathematics, Mechanics and Computer Sciences, Southern Federal University, Milchakov st., 8A, Rostov-on-Don, Russia
e-mail: solovievarc@gmail.com

Valerii Alexandrovich Chebanenko
Southern Scientific Center of Russian Academy of Science, Chekhov st., 41, Rostov-on-Don, Russia
e-mail: valera.chebanenko@yandex.ru

Ivan Anatolievich Parinov
I. I. Vorovich Institute of Mathematics, Mechanics and Computer Sciences, Southern Federal University, Milchakov st., 8A, Rostov-on-Don, Russia
e-mail: parinov_ia@mail.ru



H. Altenbach et al. (eds.), *Analysis and Modelling of Advanced Structures and Smart Systems*, Advanced Structured Materials 81,
https://doi.org/10.1007/978-981-10-6895-9_11

problems arising in different development stages of energy harvesting devices, are given in the review papers Liu et al (2009); Liao and Sodano (2009); Han et al (2013); Chebanenko et al (2015), as well as in the monographs Erturk and Inman (2011); Elvin and Erturk (2013).

PEGs are divided into two configurations: stack and cantilever. Most of the works are devoted to the study of the characteristics of cantilever type PEGs. There are several ways of modeling PEGs: a mathematical model with lumped parameters, a mathematical model with distributed parameters and a finite element model. In Dutoit et al (2005); Dutoit and Wardle (2007); Adhikari et al (2009); Roundy and Wright (2004) the focus is on the construction of PEG models based on oscillations of a mechanical system with lumped parameters. The use of such systems is a convenient modeling approach, since it allows obtaining analytical dependencies between the output parameters of PEG (potential, power, etc.) and the electrical and the mechanical characteristics as well as the resistance of the external electric circuit.

The modeling with the use of lumped parameters provides initial representations on the problem, allowing one to use simple expressions for the description of the system. However, it is approximate and restricted to only one oscillation mode. This description does not take into account important aspects of the system.

Another type of modelling is distributed parameter modeling. Based on the Euler-Bernoulli hypotheses for beams, analytical solutions of the coupled problem have been obtained in Erturk and Inman (2008); Deng et al (2014); Soloviev et al (2017) for different configurations of cantilever type PEGs. They obtained explicit expressions for the output voltage on resistive electric loads and for console displacements. In addition, the authors studied in detail behavior of PEGs with short-circuited and open-circuited electric circuits, and the influence of piezoelectric coupling effects and flexoelectric effects Deng et al (2014); Soloviev et al (2017). Nevertheless, in these studies, the case where the piezoelectric element does not completely cover the substrate has not been considered. In Nechibvute et al (2012); Soloviev et al (2013); Solovyev and Duong (2016); Yu et al (2010) the finite element modeling of the different types of cantilever PEGs are discussed. The case where the piezoelectric element does not completely cover the substrate is easily solved by this modelling approach. Nevertheless, obtaining a semi-analytical solution for the case of incomplete covering of the substrate by a piezoelectric element is of interest.

Several papers are devoted to the investigation of stack-type PEGs based on finite element modelling Feenstra et al (2008); Baker et al (2005); Cavallier et al (2005); Shevtsov et al (2016); Solovyev et al (2016) and lumped parameter modeling Dutoit et al (2005); Zhao and Erturk (2014); Goldfarb and Jones (1999). Recently, attention has been directed to analytical studies of stack type generators. Due to the fact that the stack PEGs can carry high compression levels that allows their integration in different infrastructure objects (for example, transportable roads and rail-roads. Therefore, the necessity arises to develop mathematical models for prediction of output characteristics of PEGs.

Various models of stack type PEGs have been proposed in Zhao and Erturk (2014); Wang et al (2013). The model submitted in Zhao and Erturk (2014) depends on the initial experimental data and does not provide information about displacements. The

model proposed in Wang et al (2013) does not have such disadvantages. However, it is very tedious for analysis due to its recursive type

The above brief analysis of known works has shown that the problem of modeling PEG of various configurations with the help of analytical methods in full is not yet solved, although it is quite relevant.

## 11.2 Mathematical Modelling of PEG

### *11.2.1 The Boundary-Value Problem in the Theory of Electroelasticity*

Consider a piezoelectric body of volume $V$ bounded by a surface $S$, subjected to external loads and located in an electromagnetic field. External loads include mass forces $X$ and surface loads $p$. The basic equations in the theory of electroelasticity are the equations of motion and the electric field equations (Vatulyan and Soloviev, 2009):

$$\begin{aligned} \sigma_{ji,j} + X_i &= \rho \ddot{u}_i \,, \\ D_{i,i} = 0 \,, x \in V \,, t > 0 \,, \end{aligned} \tag{11.1}$$

where $\sigma_{ij}$ denotes the components of the stress tensor, $X_i$ represents the components of the vector of mass forces, $u_i$ is a components of the displacement vector, $D_i$ stands for a component of the electric displacement vector. To these equations the constitutive laws (Vatulyan and Soloviev, 2009) are added:

$$\begin{aligned} \sigma_{ij} &= c^E_{ijkl} \varepsilon_{kl} - e_{kij} E_k \,, \\ D_i &= e_{ikl} \varepsilon_{kl} + \mathfrak{Э}^s_{ik} E_k \,, \end{aligned} \tag{11.2}$$

where $c^E_{ijkl}$ is the tensor of elastic moduli measured at a constant electric field, $\varepsilon_{kl}$ the components of the linear deformation tensor, $e_{kij}$ the tensor of piezoelectric constants, $E_k$the components of the electric field vector, and $\mathfrak{Э}^s_{ik}$ the tensor of dielectric constants measured at constant displacement. The components $\varepsilon_{kl}$ and $E_k$ are given by:

$$\begin{aligned} \varepsilon_{ij} &= \frac{1}{2}\left(u_{i,j} + u_{j,i}\right) \,, \\ E_i &= -\varphi_{,i} \,, \end{aligned} \tag{11.3}$$

where $\varphi$ electrical potential.

Substituting (11.2) and (11.3) into (11.1) we obtain a system of coupled equations in which the unknowns are the displacements $u_i$ and the electric potential $\varphi$:

$$\begin{aligned} c^E_{ijkl} u_{k,lj} + e_{kij} \varphi_{,kj} + X_i &= \rho \ddot{u}_i \,, \\ e_{ikl} u_{k,li} - \mathfrak{Э}^s_{ik} \varphi_{,ki} &= 0 \,. \end{aligned} \tag{11.4}$$

The first equation describes the motion, and the second describes the quasistatic electric field.

Mechanical and electrical boundary conditions are added to these equations (Vatulyan and Soloviev, 2009). In the case when the electrodes are connected to an external circuit, the following condition must be added:

$$\varphi|_{S_E} = v\,,$$
$$\iint\limits_{S_E} \dot{D}_i n_i ds = I\,, \tag{11.5}$$

where $S_E$ is the area of the electrode, $v$ denotes the unknown potential, which is found from the second condition, $I$ is the electric current. Thus, we have completed the formulation of the linear problem of electroelasticity.

### *11.2.2 Modeling of Cantilever Type PEGs*

We consider the functional Soloviev and Vatulyan (2011)

$$\Pi = \iiint\limits_V (H - X_i u_i)\, dV - \iint\limits_S (p_i u_i + \sigma\varphi)\, dS\,, \tag{11.6}$$

where $H$ is the electric enthalpy. The Hamiltonian principle, generalized to the theory of piezoelectricity, has the form

$$\delta \int\limits_{t_1}^{t_2} (K - \Pi)\, dt = 0\,, \tag{11.7}$$

where $K$ is the kinetic energy, and $t_2 - t_1$ stands for the time interval.

Substituting (11.6) into (11.7), we obtain the following expression for the Hamiltonian principle:

$$\int\limits_{t_1}^{t_2} dt \iiint\limits_V (\delta K - \delta H)\, dV + \int\limits_{t_1}^{t_2} dt \left[ \iiint\limits_V X_i \delta u_i dV + \iint\limits_S (p_i \delta u_i + \sigma\delta\varphi)\, dS \right] = 0\,. \tag{11.8}$$

The variation of the electric enthalpy in linear electroelasticity is:

$$\delta H = \sigma_{ij}\delta\varepsilon_{ij} - D_i \delta E_i\,. \tag{11.9}$$

The variation of the kinetic energy is

$$\delta \int_{t_1}^{t_2} K dt = -\rho \int_{t_1}^{t_2} dt \iiint_V \ddot{u}_i \delta u_i dV \,. \tag{11.10}$$

To these equations we add the constitutive equations (11.2).

Let us consider the case when there are no mass forces, external loads, and surface charge densities are applied. Then, taking into account the governing equations (11.2) and the equations (11.3), as well as the expressions for the variations (11.9) and (11.10), the Hamiltonian principle (11.8) takes the form

$$\int_{t_1}^{t_2} dt \iiint_V \left[ -\left( c_{ijkl} u_{k,l} + e_{kij} \varphi_{,k} \right) \delta u_{i,j} - \left( e_{ikl} u_{k,l} - э_{ik}\, \varphi_{,k} \right) \delta \varphi_{,i} \right] dV - \\ - \int_{t_1}^{t_2} dt \left[ \iiint_V \rho \ddot{u}_i \delta u_i dV + \iint_S \sigma \delta \varphi dS \right] = 0 \,. \tag{11.11}$$

Let us consider the simplest bimorph design of cantilever PEG, presented in Fig. 11.1. The cantilever bimorph PEG consists of two piezoelements (Fig. 11.1 points 1 and 3) glued to the substrate (Fig. 11.1 point 2), which is clamped at one end. The thickness of the electrodes and the adhesive layer, due to the smallness of their values, can be neglected.

Since this construction is nothing more than a laminated beam, to simplify the problem, we introduce the Euler-Bernoulli hypotheses The excitation of oscillations in PEGs, shown in Fig. 11.1, occurs through the movement of the base with respect to a certain plane. Therefore, the absolute displacement of the cantilever along the $x_3$ coordinate will consist of displacement of the base $w_c(t)$ and relative movement of the cantilever $w(x_1, t)$. Taking into account the foregoing, the displacement vector $u$ takes the following form:

$$u = \left\{ -x_3 \frac{\partial w(x_1, t)}{\partial x_1}, 0, w(x_1, t) - w_c(t) \right\}^T \,. \tag{11.12}$$

The transition to the consideration of the one-dimensional case also simplifies the governing equations (11.2)

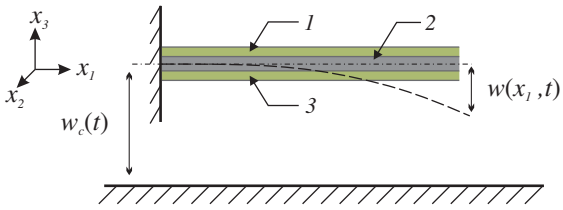


**Fig. 11.1** Bimorph cantilever PEG: 1 and 3 — piezoelements, 2 — substrate

$$\sigma_{11} = c_{11}^{E*}\varepsilon_{11} - e_{31}^{*}E_3\,,$$
$$D_3 = e_{31}^{*}\varepsilon_{11} + \mathfrak{э}_{33}^{S*}E_3\,, \tag{11.13}$$

where the material constants are expressed as follows:

$$c_{11}^{E*} = \frac{1}{s_{11}^{E}}\,,\ e_{31}^{*} = \frac{d_{31}}{s_{11}^{E}}\,,\ \mathfrak{э}_{33}^{S*} = \mathfrak{э}_{33}^{T} - \frac{d_{31}^2}{s_{11}^{E}}\,. \tag{11.14}$$

Substituting (11.12) into (11.11), taking into account (11.13) we obtain:

$$\int_{t_1}^{t_2} dt \iiint_V \left[\left(-c_{11}^{E*}x_3^2\frac{\partial^2 w(x_1,t)}{\partial x_1^2} + e_{31}^{*}x_3\varphi_{,3}\right)\delta\left(\frac{\partial^2 w(x_1,t)}{\partial x_1^2}\right)\right]dV +$$
$$+\int_{t_1}^{t_2} dt \iiint_V \left[\left(e_{31}^{*}x_3\frac{\partial^2 w(x_1,t)}{\partial x_1^2} + \mathfrak{э}_{33}^{S*}\varphi_{,3}\right)\delta\varphi_{,3}\right]dV + \tag{11.15}$$
$$+\int_{t_1}^{t_2} dt\left[\iiint_V \{-\rho(\ddot{w}(x_1,t) - \ddot{w}_c(t))\delta w(x_1,t)\}dV + \iint_S \sigma\delta\varphi dS\right] = 0\,.$$

In the PEG under investigation, the polarization vector is directed along the $x_3$ coordinate axis (see Fig. 11.2). Electrodes are applied to large sides perpendicular to the $x_3$ axis, and therefore, it makes sense to consider only the components of the electric potential along the axis $x_3$.

Since the piezoelectric element is assumed to be thin and there are no free charges inside, we suggest that the electric field is distributed linearly along the thickness of the piezoceramic element:

$$\varphi = \frac{v(t)x_3}{h}\,,\ \varphi_{,3} = \frac{v(t)}{h}\,, \tag{11.16}$$

where $v(t)$ denates the potential difference between the upper and lower electrode of the piezoelectric element, $h$ is the thickness of the piezoelectric element.

Taking into account (11.16), the expression (11.15) takes the form:

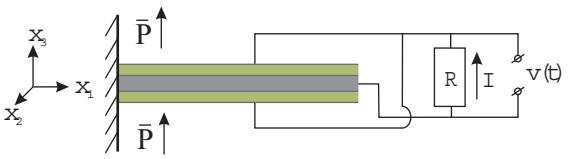


**Fig. 11.2** Wiring diagram of PEG

$$\int_{t_1}^{t_2} dt \iiint_V \left[ \left( -c_{11}^{E*} x_3^2 \frac{\partial^2 w(x_1,t)}{\partial x_1^2} + e_{31}^* x_3 \frac{v(t)}{h} \right) \delta\left( \frac{\partial^2 w(x_1,t)}{\partial x_1^2} \right) \right] dV +$$

$$+ \int_{t_1}^{t_2} dt \iiint_V \left[ \left( \frac{e_{31}^* x_3}{h} \frac{\partial^2 w(x_1,t)}{\partial x_1^2} + \ni_{33}^{S*} \frac{v(t)}{h^2} \right) \delta(v(t)) \right] dV + \quad (11.17)$$

$$+ \int_{t_1}^{t_2} dt \left[ \iiint_V \{ -\rho(\ddot{w}(x_1,t) - \ddot{w}_c(t)) \delta w(x_1,t) \} dV + \iint_S \frac{\sigma x_3}{h} \delta v(t) dS \right] = 0 .$$

To solve the problem of forced oscillations of cantilever bimorph PEGs, we will use the Kantorovich method (Kerr and Alexander, 1968). We represent the relative displacements of a beam as a series expansion:

$$w(x_1,t) = \sum_{i=1}^{N} \eta_i(t) \phi_i(x_1) , \quad (11.18)$$

where $N$ is the number of modes considered, $\eta_i(t)$ are the unknown generalized coordinates, $\phi_i(x_1)$ denotes the known test functions that satisfy the boundary conditions.

Substituting the representation (11.18) in (11.17) and equating the coefficients with independent variations of $\delta v$ and to zero $\delta \eta$, we obtain a system of differential equations describing the forced oscillations of the bimorph PEG connected to the resistor:

$$M\ddot{\eta}(t) + D\dot{\eta}(t) + K\eta(t) - \Theta v(t) = p,$$
$$C_p v(t) + \Theta^T \eta(t) = -q , \quad (11.19)$$

where $D = \mu M + \gamma K$ is the Rayleigh-type damping matrix, and the remaining coefficients are:

$$
\begin{aligned}
C_p &= \frac{bL}{h}\, э_{33}^{S*}, \\
M_{ij} &= \int_0^L m\phi_i(x_1)\phi_j(x_1)dx_1, \\
K_{ij} &= \int_0^L EI\phi_i''(x_1)\phi_j''(x_1)dx_1, \\
p_i &= -\ddot{w}_c(t)\int_0^L m\phi_i(x_1)dx_1, \\
\theta_i &= \int_0^L J_p\phi_i''(x_1)dx_1\ ,
\end{aligned}
\tag{11.20}
$$

where $C_p$ is the electric capacity, $M_{ij}$ denotes the elements of the mass matrix, $K_{ij}$ are the elements of the stiffness matrix, $\theta_i$ represents the elements of the electromechanical coupling vector, $p_i$ are the elements of the effective mechanical load vector, $m$ is the specific weight, $EI$ stands for the bending stiffness, $M$ denotes the proof mass.

Differentiating with time the second equation in system (11.19), taking into account the fact that $\dot{q} = I$, we will satisfy condition (11.5). Using Ohm's law, we obtain the equation for the electric circuit in the following form:

$$
C_p\dot{v}(t) + \Theta^T\dot{\eta}(t) + \frac{v(t)}{R} = 0\,, \tag{11.21}
$$

where $R$ is the electrical resistance (the resistor on which the voltage is measured see Fig. 11.2).

Figure 11.1 shows the simplest case of a bimorph cantilever PEG, but in reality the production of such a structure is rather difficult. It becomes necessary to take into account such design features as incomplete covering of the piezoelectric element of the substrate. In addition, to adjust the resonance frequency and increase the output power, proof mass is often used. In view of the foregoing, we will consider the PEG shown in Fig. 11.3. Hereinafter, the subscripts $p$, $s$ and $m$ will denote that the variable corresponds to the piezoelectric element, substrate and mass, respectively.

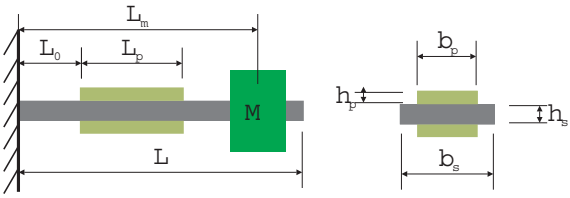


**Fig. 11.3** Bimorph cantilever PEG with piezoelement and proof mass displaced relative to the clamp

The search for a solution for this design is associated with the need to divide the beam into four segments. The first segment begins at the clamp and contains to the beginning of the piezoelement. The second segment is the part of the substrate covered with a piezoelectric element. The third segment is the free part of the beam, following the piezoelement up to the attachment point of the proof mass (mass is considered as a point). The fourth segment starts right after the proof mass and contains to the end of the beam. Taking into account the division of the beam described above, the piecewise-defined function $\phi_i(x_1)$ takes the following form:

$$\phi_i(x_1) = \begin{cases} \phi_i^{(1)}(x_1), x_1 \le L_0 \\ \phi_i^{(2)}(x_1), L_0 < x_1 \le L_p + L_0 \\ \phi_i^{(3)}(x_1), L_p + L_0 < x_1 \le L_m \\ \phi_i^{(4)}(x_1), x_1 > L_m \end{cases}, \tag{11.22}$$

where $\phi_i^{(1)}$, $\phi_i^{(2)}$, $\phi_i^{(3)}$, $\phi_i^{(4)}$ correspond to the modes of oscillation of the first, second, third and fourth segments, respectively. We write the solution in a general form for each part of the beam:

$$\begin{aligned} \phi_i^{(1)}(x_1) &= a_{1,i}\sin(\beta_i x_1) + a_{2,i}\cos(\beta_i x_1) + a_{3,i}\sinh(\beta_i x_1) + a_{4,i}\cosh(\beta_i x_1) \\ \phi_i^{(2)}(x_1) &= a_{5,i}\sin(\beta_i x_1) + a_{6,i}\cos(\beta_i x_1) + a_{7,i}\sinh(\beta_i x_1) + a_{8,i}\cosh(\beta_i x_1) \\ \phi_i^{(3)}(x_1) &= a_{9,i}\sin(\beta_i x_1) + a_{10,i}\cos(\beta_i x_1) + a_{11,i}\sinh(\beta_i x_1) + a_{12,i}\cosh(\beta_i x_1) \\ \phi_i^{(4)}(x_1) &= a_{13,i}\sin(\beta_i x_1) + a_{14,i}\cos(\beta_i x_1) + a_{15,i}\sinh(\beta_i x_1) + a_{16,i}\cosh(\beta_i x_1) \ . \end{aligned} \tag{11.23}$$

Next, we write down the boundary conditions:

$$\phi_i^{(1)}(0) = 0\,, \phi_i'^{(1)}(0) = 0\,, \quad \phi_i''^{(4)}(L) = 0\,, \phi_i'''^{(4)}(L) = 0\,. \tag{11.24}$$

In addition, we will need the conjugation conditions for the beam segments:

$$
\begin{aligned}
\phi_i^{(1)}(L_0) &= \phi_i^{(2)}(L_0)\\
\phi_i^{'(1)}(L_0) &= \phi_i^{'(2)}(L_0)\\
\phi_i^{''(1)}(L_0) &= \frac{EI^{(2)}}{EI^{(1)}}\phi_i^{''(2)}(L_0)\\
\phi_i^{'''(1)}(L_0) &= \frac{EI^{(2)}}{EI^{(1)}}\phi_i^{'''(2)}(L_0)\\
\phi_i^{(2)}\left(L_0+L_p\right) &= \phi_i^{(3)}\left(L_0+L_p\right)\\
\phi_i^{'(2)}\left(L_0+L_p\right) &= \phi_i^{'(3)}\left(L_0+L_p\right)\\
\phi_i^{''(2)}\left(L_0+L_p\right) &= \frac{EI^{(1)}}{EI^{(2)}}\phi_i^{''(3)}\left(L_0+L_p\right)\\
\phi_i^{'''(2)}\left(L_0+L_p\right) &= \frac{EI^{(1)}}{EI^{(2)}}\phi_i^{'''(3)}\left(L_0+L_p\right)\\
\phi_i^{(3)}(L_m) &= \phi_i^{(4)}(L_m)\\
\phi_i^{'(3)}(L_m) &= \phi_i^{'(4)}(L_m)\\
\phi_i^{''(3)}(L_m) &= \phi_i^{''(4)}(L_m)\\
\phi_i^{'''(3)}(L_m) &= \phi_i^{'''(4)}(L_m) - \alpha\beta^4\phi_i^{(3)}(L_m)\\
\alpha &= \frac{M}{mL}\,,
\end{aligned}
\tag{11.25}
$$

where $EI^{(1)}$ and $EI^{(2)}$ are bending stiffness of segments.

Adding a proof mass to the model requires considering its effect on the system of equations (11.19), since it is an additional inertial load that affects the kinetic energy. Taking into account the proof mass, the expressions for some components of (11.20) change as follows:

$$
\begin{aligned}
M_{ij} &= \int_0^L m\phi_i(x_1)\phi_j(x_1)dx_1 + M\phi_i(L_m)\phi_j(L_m),\\
p_i &= -\ddot{w}_c(t)\int_0^L m\phi_i(x_1)dx_1 + M\phi_i(L_m)\,.
\end{aligned}
\tag{11.26}
$$

Satisfying the boundary conditions, we obtain a homogeneous system of 16 equations with 16 unknowns:

$$
\Lambda = \begin{pmatrix} a_{1,1} & \dots & a_{1,16}\\ \vdots & \ddots & \vdots\\ a_{16,1} & \cdots & a_{16,16}\end{pmatrix},
\tag{11.27}
$$

The specific weight $m(x_1)$, for the case under consideration, is calculated as follows:

$$m(x_1) = \rho_s A_s + 2\rho_p A_p \Big(H(x_1 - L_0) - H(x_1 - L_0 - L_p)\Big) , \tag{11.28}$$

where $H(x_1)$ is the Heaviside function.

The bending stiffness $EI$ for the model under consideration is calculated as follows:

$$EI(x_1) = c_p \left[ \iint\limits_{S_{p1}} x_3^2 dS + \iint\limits_{S_{p2}} x_3^2 dS \right] \Big(H(x_1 - L_0) - H(x_1 - L_0 - L_p)\Big) + c_s \iint\limits_{S_s} x_3^2 dS , \tag{11.29}$$

where $c_p$ and $c_s$ are elastic constants of piezoelements and substrate, respectively, $S_{p1}$, $S_{p1}$ and $S_s$ are cross-section areas of upper and lower piezoelements and substrate, respectively. The function $J_p(x_1)$ is equal to

$$J_p(x_1) = \frac{e_{31}^*}{h_p} \left( \iint\limits_{S_{p1}} x_3 dS + \iint\limits_{S_{p2}} x_3 dS \right) \Big(H(x_1 - L_0) - H(x_1 - L_0 - L_p)\Big) . \tag{11.30}$$

After all the preliminary steps have been taken, we proceed directly to solving the system of equations (11.19). We assume that the excitation is harmonic:

$$\begin{aligned} w_c(t) &= \tilde{w}_c e^{i\omega t} \\ p &= \tilde{p} e^{i\omega t} . \end{aligned} \tag{11.31}$$

Then we seek the solution in the form

$$\begin{aligned} \eta(t) &= \tilde{\eta} e^{i\omega t} \\ v(t) &= \tilde{v} e^{i\omega t} . \end{aligned} \tag{11.32}$$

A tilde above a variable indicates the amplitude. After substituting (11.31) and (11.32), the system of equations (11.19) takes the form

$$\begin{aligned} \Big[-\omega^2 M + i\omega(\mu M + \gamma K) + K\Big]\tilde{\eta} - \Theta\tilde{v} &= \tilde{p}, \\ \left(i\omega C_p + \frac{1}{R}\right)\tilde{v} + i\omega\Theta^T\tilde{\eta} &= 0 . \end{aligned} \tag{11.33}$$

From the second equation in system (11.33) we obtain $\tilde{v}$

$$\tilde{v} = -\frac{i\omega\Theta^T\tilde{\eta}}{i\omega C_p + \frac{1}{R}} . \tag{11.34}$$

Then we substitute (11.34) into the first equation of the system (11.32) and express $\tilde{\eta}$

$$\tilde{\eta} = \left[ -\omega^2 M + i\omega(\mu M + \gamma K) + K + \frac{i\omega\Theta\Theta^T}{i\omega C_p + \frac{1}{R}} \right]^{-1} \tilde{p} . \tag{11.35}$$

Substituting expression for $\tilde{\eta}$ back into (11.34), we get a new expression for $\tilde{v}$

$$\tilde{v} = -\frac{i\omega\Theta^T}{i\omega C_p + \frac{1}{R}}\left[-\omega^2 M + i\omega(\mu M + \gamma K) + K + \frac{i\omega\Theta\Theta^T}{i\omega C_p + \frac{1}{R}}\right]^{-1}\tilde{p}\,. \tag{11.36}$$

The obtained expressions (11.35) and (11.36) are solutions of the system of equations (11.33).

#### 11.2.2.1 Numerical Experiment

We will consider a bimorph cantilever PEG, manufactured using the PKR-7M ceramic, which has the geometric and physical properties given in Table 11.1. The excitation of the system is given by a harmonic displacement of the base $w_c = \tilde{w}_c e^{i\omega t}$, whose amplitude is $\tilde{w}_c = 0.1$ mm, and the coefficients of the modal damping are equal $\xi_1 = \xi_2 = 0.02$.

The first step in the research is the construction of amplitude-frequency characteristics (AFC) of displacements, potentials arising on electrodes, etc. Figure 11.4 shows the frequency response of the voltage, on the external electrodes, and the displacement of the end of the beam. In the literature (Erturk and Inman, 2011; Elvin and Erturk, 2013), the main performance characteristics of PEGs are the dependence of voltage and power on electrical resistance. Here are dependencies of the main characteristics of the PEG on the electrical resistance. All characteristics were investigated at the first resonant frequency.

Figure 11.5 is a typical dependence of the output electric voltage on electrical resistance. With increasing resistance, the voltage rises to a certain limiting value. This limit value corresponds to the open circuit condition.

The output power is calculated by the formula:

$$P = \frac{v^2}{R}\,. \tag{11.37}$$

Table 11.1: PEG Parameters

| | Substrate | Piezoelement |
|---|---|---|
| Geometrical dimensions ($L_0 \times b \times h$) | 110×10×1 mm$^3$ | 56×6×0.5 mm$^3$ |
| Density ($\rho$) | 1650 kg/m$^3$ | 8000 kg/m$^3$ |
| The Young's modulus and Poisson's ratio ($E, \nu$) | 15 GPa and 0.12 | — |
| Elastic compliance $\left(s_{11}^E\right)$ | — | 17.5×10$^{-12}$ Pa |
| Relative permittivity $\left(\varepsilon_{33}^S/\varepsilon_0\right)$ | — | 5000 |
| Piezoelectric module ($d_{31}$) | — | -350 pC/N |

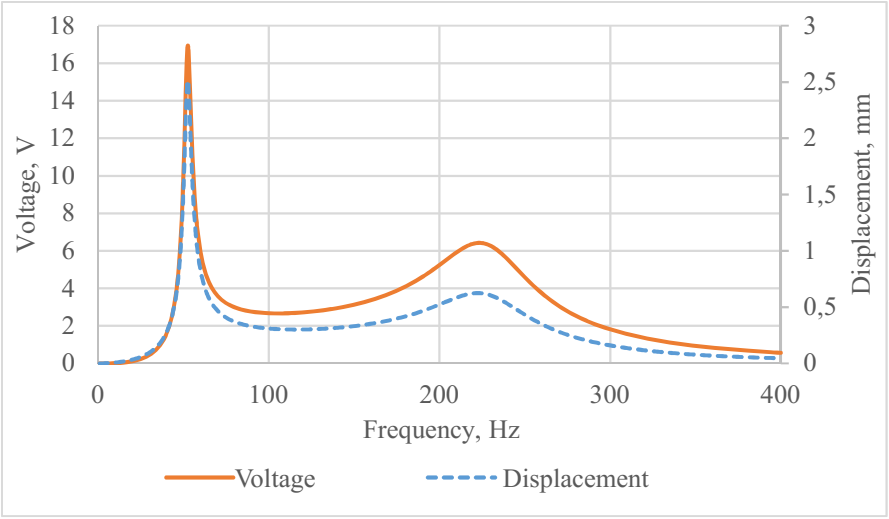


**Fig. 11.4**: Amplitude-frequency response of the voltage and the displacement of the beam's end

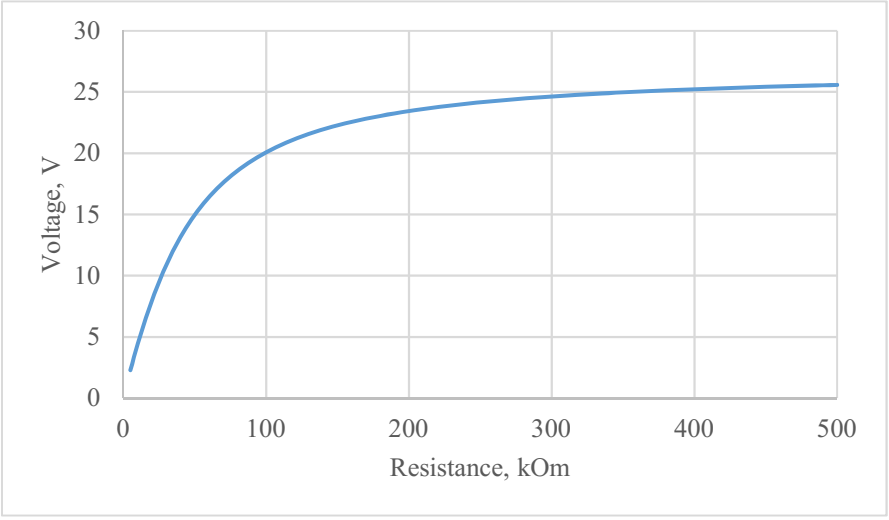


**Fig. 11.5**: Dependence of voltage on electrical resistance

In addition to the dependence of the output power on the electrical resistance, we shall construct the dependence of the displacement of the end of the beam on the electrical resistance.

Figure 11.6 shows a typical dependence of output power on electrical resistance. This dependence for power is characterized by the presence of a maximum, the

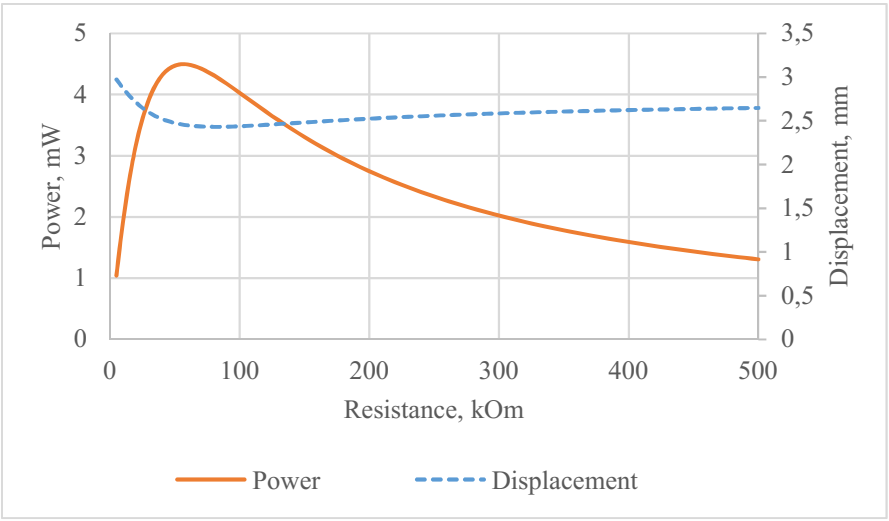


**Fig. 11.6**: Dependencies of output power and displacement of the beam's end from resistance

position of which depends on the electrical capacity of the piezoelements and the excitation frequency of the PEG. The dependence of the displacement of the free end of the beam on the electrical resistance has a minimum, the position of which coincides with the maximum of power. This indicates that the conversion of mechanical energy into electrical energy, at a given value of electrical resistance, is maximized.

#### 11.2.2.2 Comparison with Finite Element

In the literature there are mathematical models of PEGs with lumped parameters. They are convenient for describing the stack type PEGs. In the case of generators of the cantilever type, they give inaccurate results. There is work in which corrective coefficients for these models are given, but they are suitable for the case when the piezoelectric element completely covers the surface of the substrate. In the case of incomplete coverage, preliminary experiments are required to identify the parameters of the five model parameters. This is the obstacle to design. Therefore, we compare the obtained mathematical model with a finite element model (cf. Fig. 11.7).

Soloviev et al (2013) deals with the finite element modeling of the laboratory model of cantilever PEG. The calculation was made for the cantilever model described at the beginning of previous paragraph. The value of the proof mass was 5 g.

Measurements were made in conditions of an open circuit when the cantilever base was excited by a displacement of 0.1 mm. Dependencies for the first resonant frequencies and the output electric potential were obtained, depending on the thick-

**Fig. 11.7** Finite element model in ANSYS

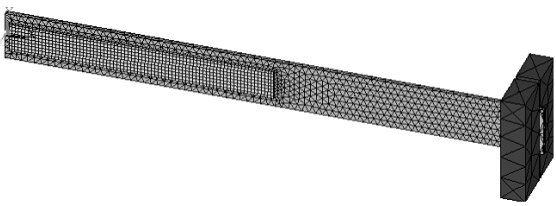

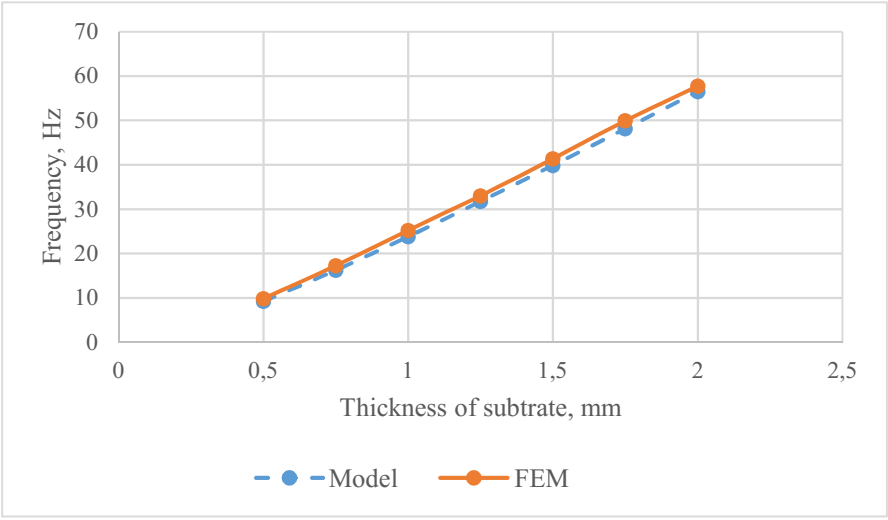


**Fig. 11.8**: Dependence of the first resonance frequency on the thickness of the substrate: dashed line —- model, solid — finite element simulation

ness of the substrate. We perform similar calculations and compare the obtained data.

As can be seen from Fig. 11.8 with increasing substrate thickness, the value of the first resonant frequency also increases. The difference between the finite element calculation and the model does not exceed 5%, which indicates a sufficient accuracy of the constructed model.

From Fig. 11.9, it follows that as the thickness of the substrate increases, the value of the output electric potential increases. The difference between the finite element calculation and the model does not exceed 7%, which indicates a sufficient accuracy of the constructed model.

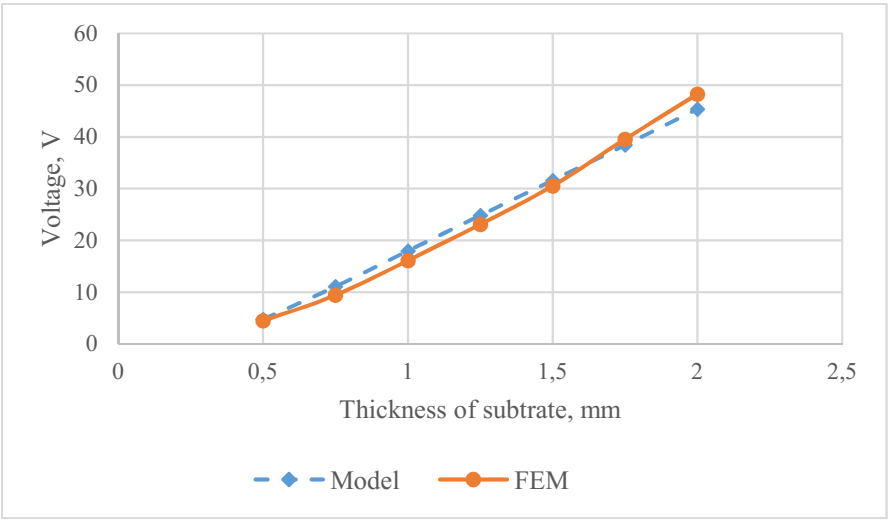


**Fig. 11.9**: Dependence of the output electric potential on the thickness of the substrate: dashed line — model, solid line — finite element simulation

#### 11.2.2.3 Parametric Studies

Next, we will investigate the dependencies of the main performance characteristics of cantilever PEGs (resonance frequency, beam tip's displacement, output voltage and power) on the position of the proof mass, and the position of the piezoelement.

Consider the effect of the position of the proof mass $M$ of 3 g on the performance of the PEG. As the main parameter we will use the relative position of the proof mass, i.e. normalized with respect to the coordinate of the end of the substrate.

As can be seen from Fig. 11.10 with increasing distance between clamped end and the proof mass, the first resonance frequency of the beam decreases. From Fig. 11.11 we can conclude that at some position of the proof mass, the maximum displacement of the end of the beam is achieved. From Fig. 11.12 it follows that at some position of the proof mass, there are local maxima of the output voltage and the maximum of the output power (with the optimum electrical resistance). Since the power directly depends on the electrical resistance, it makes sense to consider the value of the resistance at which power is maximal i.e. optimum electrical resistance. Figure 11.13 demonstrates that the closer the proof mass is to the end of the beam, the higher the value of the optimum electrical resistance. Analyzing the obtained data, we can conclude that there is a certain value of the position of the proof mass, at which the maximum output power is reached.

Next, we consider the case when the length of the piezoelement is fixed. We will investigate the effect of repositioning of the piezoelectric element relative to the clamped end on the performance of the PEG, taking into account the presence of the proof mass of 3 g. As the main parameter, we will use the relative offset, i.e.

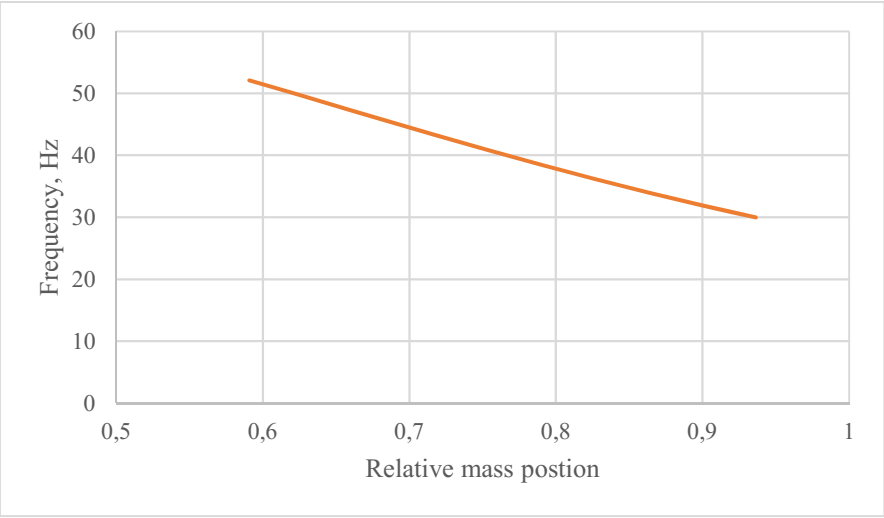


**Fig. 11.10**: Dependence of the first resonance frequency on the position of the proof mass

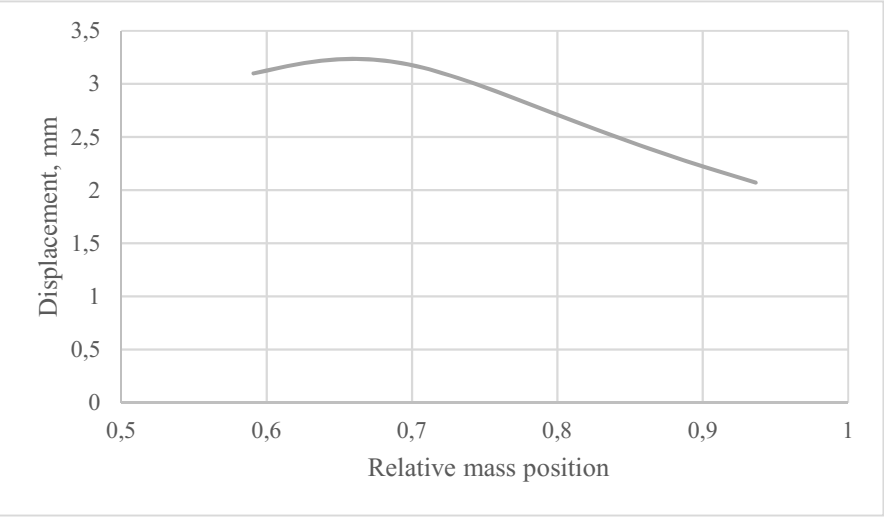


**Fig. 11.11**: Dependence of the displacement of the beam's end on the position of the proof mass

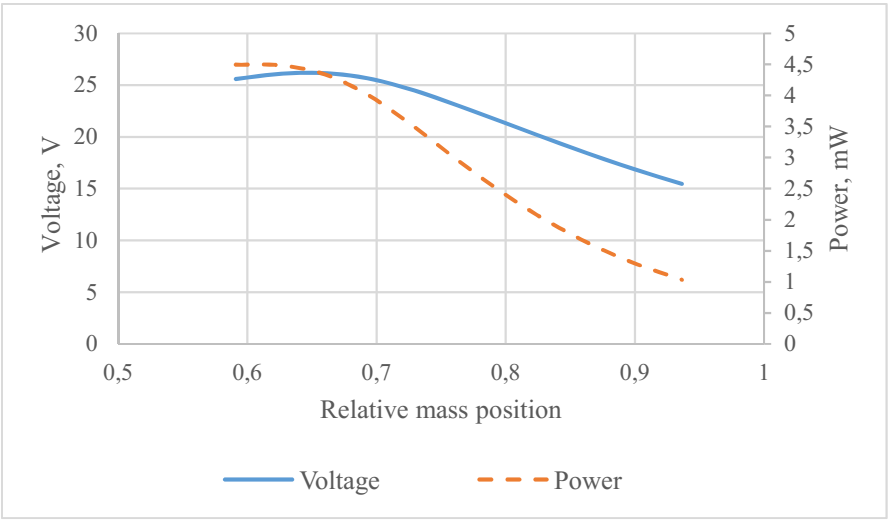


**Fig. 11.12**: Dependence of the maximum output voltage and power on the position of the proof mass

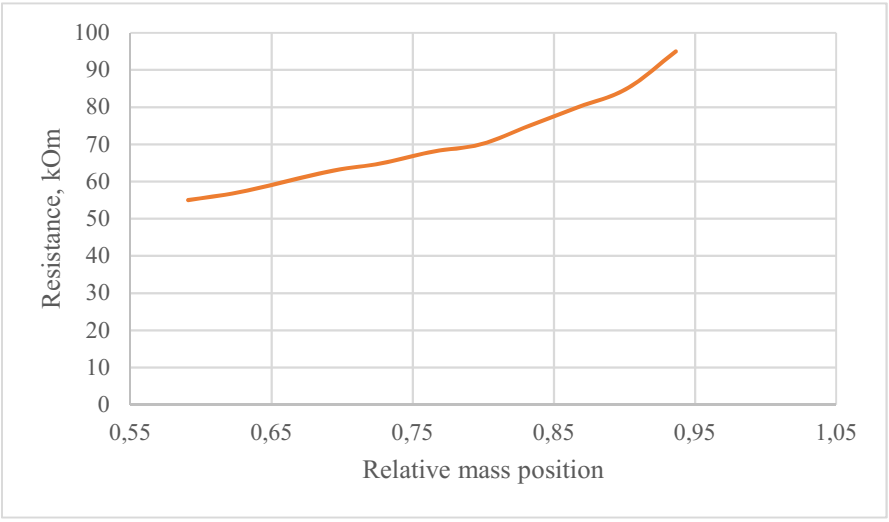


**Fig. 11.13**: Dependence of the resistance value at which the maximum power is reached, from the position of the proof mass

normalized with respect to the length of the substrate. This parameter is responsible for the coordinate of the beginning of the piezoelement. From Fig. 11.14 it can be seen that as the position of piezoelectric element becomes more indented, the first resonance frequency decreases monotonically. Figure 11.15 shows that with

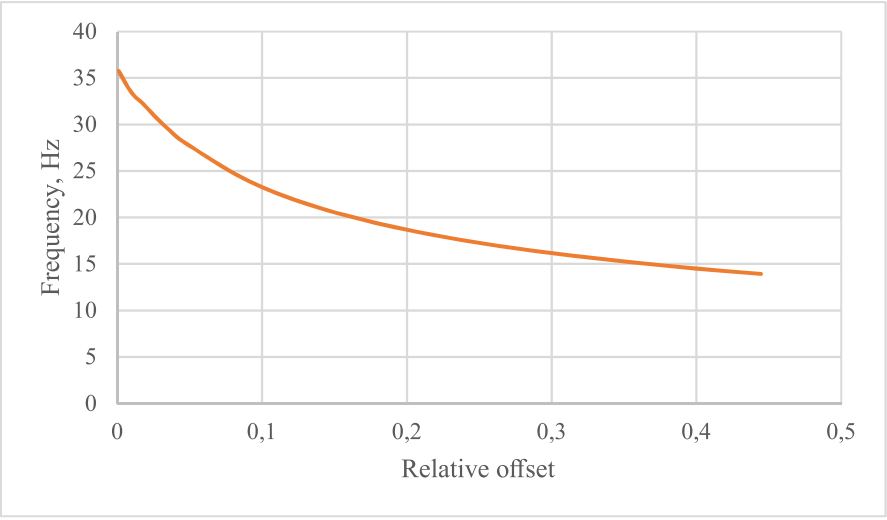


**Fig. 11.14**: Dependence of the first resonance frequency on the offset from clamp

increasing offset of the piezoelectric element from the clamp displacement of the end of the beam decreases slightly at a small interval, and then increases. This may indicate that the bending stiffness of the beam near the clamping zone decreases. In Fig. 11.16 it is shown that with an increase in the piezoelectric element's offset from the clamped end, the output voltage drops noticeably. Moreover, the maximum voltage is observed when the offset is minimal. The maximum output power demonstrates similar behavior. The dependence of the value of the electrical resistance, at which the maximum power is reached, on the amount of offset of the piezoelectric element from the clamped end, depicted in Fig. 11.17, has a monotonous increasing character. The obtained data on the influence of the position of the piezoelectric element on the output characteristics of the PEG indicate that it is most advantageous from the point of view of obtaining maximum power to position the piezoelectric element near the clamp.

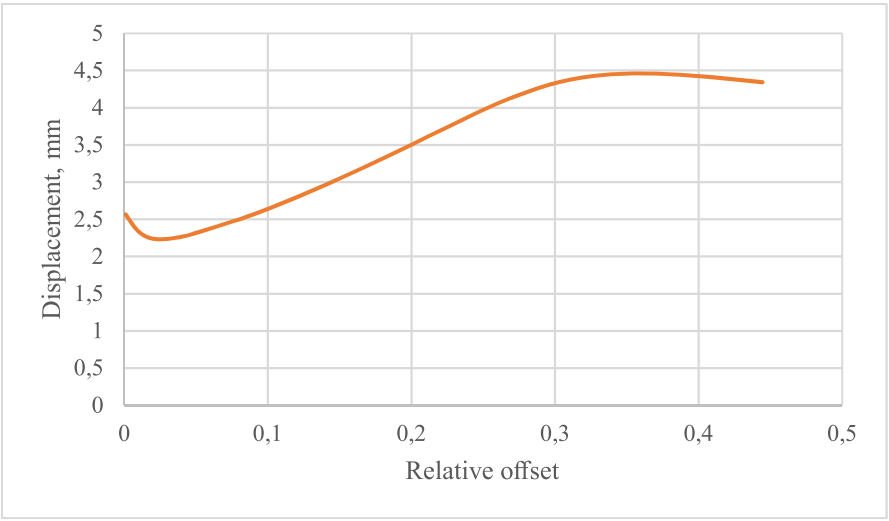


**Fig. 11.15**: Dependence of the displacement of the beam's end on the position of the piezoelectric element

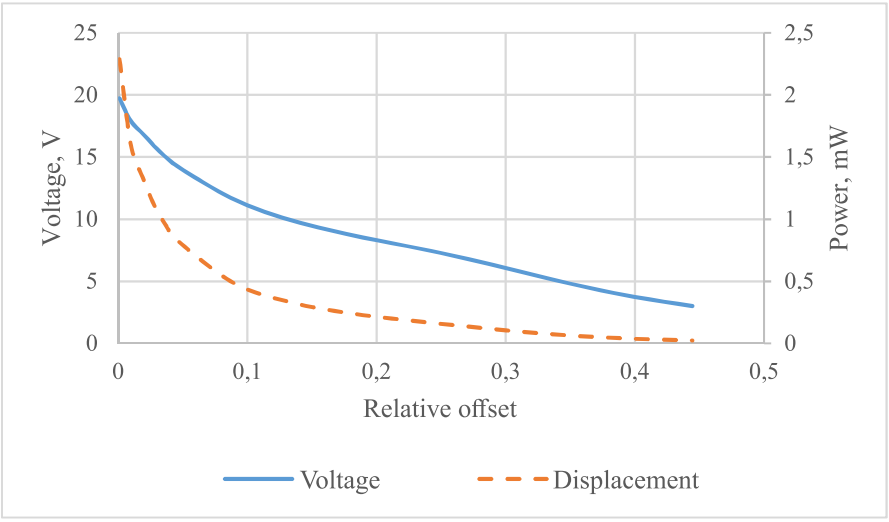


**Fig. 11.16**: Dependence of the maximum output voltage and power on the amount of indentation of the piezoelectric element from the termination

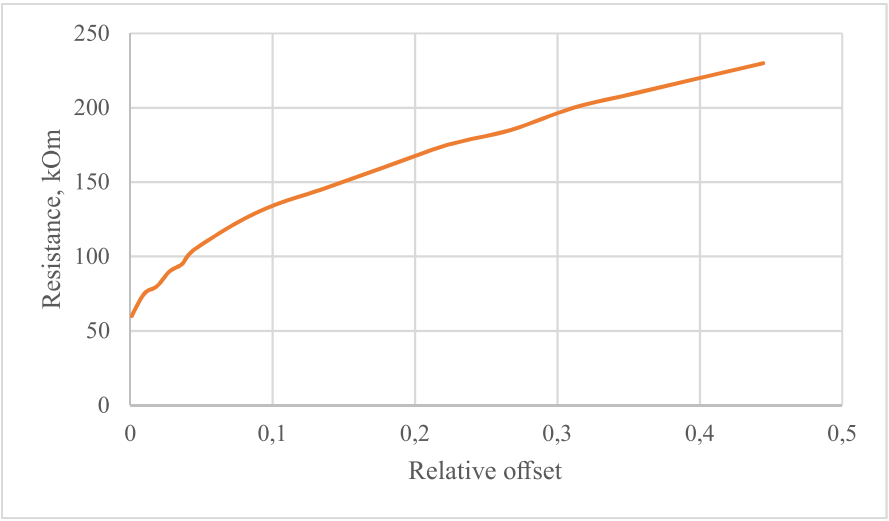


**Fig. 11.17**: Dependence of the resistance value, at which the maximum power is reached, on the offset from clamp

### *11.2.3 Modelling of Stack Type PEG*

The derivation of the equations describing the behavior of the stack-type PEG, shown in Fig. 11.18, is also based on the Hamiltonian principle given earlier. This PEG is subjected to an external mechanical loading $p(t)$ along the coordinate axis $x_3$.

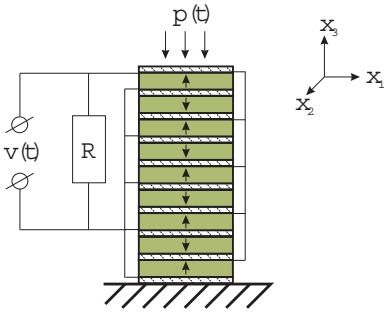


**Fig. 11.18** Stack PEG scheme

Therefore, repeating the calculations (11.6)–(11.11), we obtain the following equation:

$$\int_{t_1}^{t_2} dt \iiint_V \left[-\left(c_{ijkl}u_{k,l}+e_{kij}\varphi_{,k}\right)\delta u_{i,j}-\left(e_{ikl}u_{k,l}-\ni_{ik}\,\varphi_{,k}\right)\delta\varphi_{,i}\right]dV- \\ -\int_{t_1}^{t_2} dt\left[\iiint_V \rho\ddot{u}_i\delta u_i dV+\iint_S (p_i\delta u_i+\sigma\delta\varphi)\,dS\right]=0\,, \tag{11.38}$$

where, in contrast to (11.11), external loads $p_i$ are conserved.

Let us consider the construction of PEGs of the stack type, shown in Fig. 11.18. The simplest stacked PEG consists of several piezoceramic plates connected to each other (either glued at the production stage, or stapled mechanically). The thickness of the electrodes can, due to the smallness of its values, be neglected.

After introducing the assumption of small deformations, the problem reduces to forced longitudinal vibrations of the rod along the $x_3$ coordinate. Taking into account the foregoing, the displacement vector $u$ takes the following form:

$$u=\{0,0,w(x_3,t)\}^{\mathrm{T}}\,. \tag{11.39}$$

The transition to the consideration of the one-dimensional case also simplifies the governing equations (11.2):

$$\sigma_{11}=c_{33}^{E*}\varepsilon_{33}-e_{33}^{*}E_3\,, \\ D_3=e_{33}^{*}\varepsilon_{33}+\ni_{33}^{S*}E_3\,, \tag{11.40}$$

where the material constants are expressed as follows:

$$c_{33}^{E*}=\frac{1}{s_{33}^{E}}\,,\ e_{33}^{*}=\frac{d_{33}}{s_{33}^{E}}\,,\ \ni_{33}^{S*}=\ni_{33}^{\mathrm{T}}-\frac{d_{33}^{2}}{s_{33}^{E}}\,. \tag{11.41}$$

Substituting (11.39) into (11.38), taking into account (11.40), we obtain:

$$\int_{t_1}^{t_2} dt \iiint_V \left[\left(-c_{33}^{E*}\frac{\partial w(x_3,t)}{\partial x_3}+e_{33}^{*}\varphi_{,3}\right)\delta\left(\frac{\partial w(x_3,t)}{\partial x_3}\right)\right]dV+ \\ +\int_{t_1}^{t_2} dt \iiint_V \left[\left(e_{33}^{*}\frac{\partial w(x_3,t)}{\partial x_3}+\ni_{33}^{S*}\varphi_{,3}\right)\delta\varphi_{,3}\right]dV+ \\ +\int_{t_1}^{t_2} dt\left[\iiint_V \{-\rho\ddot{w}(x_3,t)\delta w(x_3,t)\}\,dV+\iint_S (p_3\delta w(x_3,t)+\sigma\delta\varphi)\,dS\right]=0\,. \tag{11.42}$$

In the studied PEG, the polarization vector is directed along the coordinate axis $x_3$. The electrodes are applied to the long sides of piezoceramic plates perpendicular to the axis $x_3$. They are connected in parallel (see Fig. 11.18). Accordingly, it makes

sense to consider only the components of the electric potential gradient along the axis $x_3$.

Since the piezoelements are assumed to be thin and there are no free charges inside, we assume that the electric field is distributed linearly along the thickness of each piezoceramic element:

$$\varphi = \frac{v(t)x_3}{h}\,,\ \varphi_{,3} = \frac{v(t)}{h}\,, \tag{11.43}$$

where $v(t)$ is the potential difference between the upper and lower electrode of the piezoelectric element, $h$ denotes the thickness of the single piezoelectric layer. Taking into account (11.43), the expression (11.41) takes the form:

$$\begin{aligned}
&\int_{t_1}^{t_2} dt \iiint_V \left[\left(-c_{33}^{E*}\frac{\partial w(x_3,t)}{\partial x_3} + e_{33}^{*}\frac{v(t)}{h}\right)\delta\left(\frac{\partial w(x_3,t)}{\partial x_3}\right)\right] dV + \\
&\quad + \int_{t_1}^{t_2} dt \iiint_V \left[\left(\frac{e_{33}^{*}}{h}\frac{\partial w(x_3,t)}{\partial x_3} + \ni_{33}^{S*}\frac{v(t)}{h^2}\right)\delta v(t)\right] dV + \\
&+ \int_{t_1}^{t_2} dt \left[\iiint_V \{-\rho\ddot{w}(x_3,t)\delta w(x_3,t)\}\, dV + \iint_S \left(p_3\delta w(x_3,t) + \frac{\sigma x_3}{h}\delta v(t)\right) dS\right] = 0\,.
\end{aligned} \tag{11.44}$$

To solve the problem of forced longitudinal oscillations of stacked PEGs, we will also use the Kantorovich method. Further, repeating the calculations similarly to the derivation of equations (11.18)–(11.21), we obtain a system of differential equations describing the forced oscillations of the stacked PEG connected to the resistor:

$$\begin{aligned}
M\ddot{\eta}(t) + D\dot{\eta}(t) + K\eta(t) - \Theta v(t) &= p, \\
C_p\dot{v}(t) + \Theta^T\dot{\eta}(t) + \frac{v(t)}{R} &= 0\,.
\end{aligned} \tag{11.45}$$

Coefficients of (11.45) are equal to:

$$
\begin{aligned}
C_p &= N_p \frac{bl}{h} \ni_{33}^{S*}, \\
M_{ij} &= \int_0^H m\phi_i(x_3)\phi_j(x_3)dx_3, \\
K_{ij} &= \int_0^H Y\phi_i'(x_3)\phi_j'(x_3)dx_3, \\
p_i &= -p_0\phi_i(x_3), \\
\theta_i &= \int_0^H J_p\phi_i'(x_3)dx_3, \\
Y &= \iint_S c_{33}^{E*}dS, \\
J_p &= \iint_S \frac{e_{33}^*}{h}dS\ ,
\end{aligned}
\tag{11.46}
$$

where $N_p$ is the number of piezoelectric layers, $b$, $l$ and $h$ are the width, length and height of single piezoelement, $H$ denotes the height of the whole stack, $Y$ stands for the rigidity of the cross section of the stack.

Now it remains to find a set of test functions satisfying the boundary conditions. The search for test functions satisfying the boundary conditions is connected to the solution of the eigenvalue problem for the rod. We solve the problem of free vibrations of the rod shown in Fig. 11.18. Let us write out the solution in general form:

$$\phi_i(x_3) = a_{1,i}\sin(\beta_i x_3) + a_{2,i}\cos(\beta_i x_3)\ . \tag{11.47}$$

Boundary conditions in the considered case are:

$$\phi_i(0) = 0\ ,\ \phi_i'(H) = 0\ . \tag{11.48}$$

We can find the eigenvalues $\beta_i$ and coefficients $a_i$.

After this we obtain a homogeneous system of 4 equations with 4 unknowns which is given in matrix form:

$$\Lambda = \begin{pmatrix} a_{1,1} & \cdots & a_{1,4} \\ \vdots & \ddots & \vdots \\ a_{4,1} & \cdots & a_{4,4} \end{pmatrix} = 0\ . \tag{11.49}$$

This system has nonzero solutions when its determinant is zero. The determinant of the system yields a characteristic equation that needs to solve in order to compute the eigenvalues $\beta_i$:

$$1 + \cos\beta_i \cosh\beta_i = 0\ . \tag{11.50}$$

Equation (11.50) is transcendental. Therefore we will solve it with numerical methods. Knowing $\beta_i$, we can find the coefficients $a_i$ for the required number of vibration modes $N$.

For the case of harmonic loading, obtaining the solution of the system (11.45) is analogous to the solution for harmonic loading of the cantilever PEG (11.31)-(11.36). Here, the loading of an arbitrary shape, in particular the impulse form, will be considered.

To consider a load $p(t)$ having an arbitrary shape, we represent its amplitude values with a set of discrete values, and then interpolate it using Fourier series:

$$p(t) \cong m_0 + \sum_{k=1}^{N} \left[ m_k \cos\left(k\frac{2\pi t}{T}\right) + n_k \sin\left(k\frac{2\pi t}{T}\right) \right], \tag{11.51}$$

where $m_0$ is the average value, $T$ denotes the loading duration, $n_k, m_k$ are Fourier coefficients.

$$m_0 = \frac{1}{T}\int_0^T p(t)dt,\ m_k = \frac{2}{T}\int_0^T p(t)\cos\left(k\frac{2\pi t}{T}\right)dt,\ n_k = \frac{2}{T}\int_0^T p(t)\sin\left(k\frac{2\pi t}{T}\right)dt\,. \tag{11.52}$$

Then, we substitute the obtained approximation (11.51) into (11.45) and solve the system numerically by the Runge-Kutta method.

### 11.2.3.1 Parametric Studies

As input parameters of the model, we use the initial data from the experiment. We will consider stack PEG, made using disk elements from ceramics PZT-19. The model of PEG considered in Fig. 11.19, is a stack of piezoelements of the ring type, connected together by a coupling bolt. Above and below are metal discs that distribute the

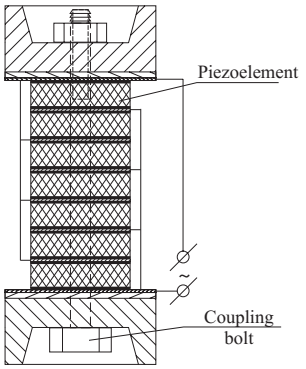


**Fig. 11.19** Schematic model of the stacked PEG

applied load evenly over the section, and protect against direct mechanical action

on the piezoelements. The metal discs are followed by an insulating spacer, which prevents electrical shorting. Between the piezoelements are located electrodes. They are connected in parallel. In order to take into account the influence of the metal core (clamping bolt) in the cross section of the PEG, we add to the rigidity of the cross section $Y$ one more term:

$$Y = \iint\limits_{S_p} c_{33}^{E*} dS + \iint\limits_{S_c} c_c dS \ , \tag{11.53}$$

where $S_p$ and $S_c$ are the areas of the section of the stack and bolt, respectively, $c_{33}^{E*}$ and $c_c$ represent the modulus of elasticity of the piezoceramic and steel, respectively.

This PEG will be subjected to a pulsed loading, the shape of which is shown in Fig. 11.20. The main geometric and physical properties of the generator model

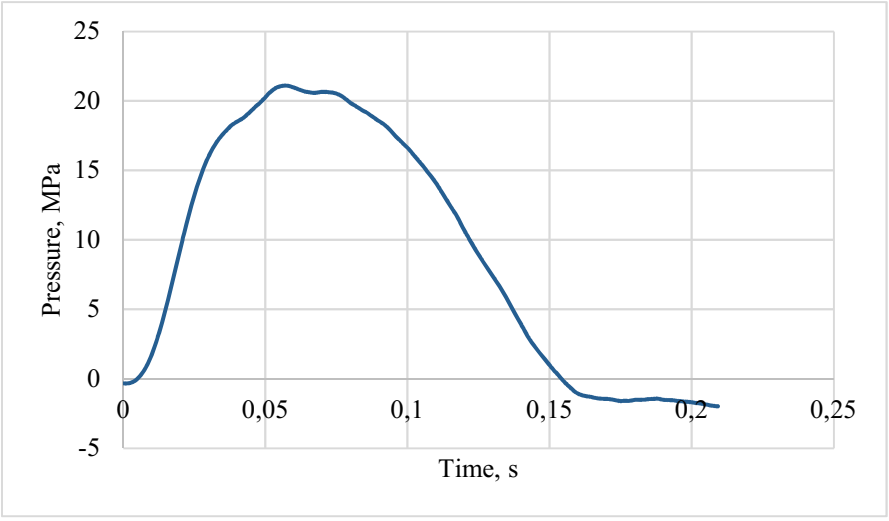


**Fig. 11.20**: Shape of the loading force

under study are given in Table 11.2. The modal damping coefficients are equal $\xi_1 = \xi_2 = 0.02$.

Investigations of the dependence of the main characteristics of the stacked PEG (output voltage and power) on various parameters (geometric sizes of piezoelements and the number of piezoelements) were carried out. Figure 11.21 shows the dependence of the maximum output voltage and the power on the number of layers of PEG. The geometry of the layers is assumed to be unchanged. From the above dependence, it follows that with an increase in the number of layers, the output voltage and power increase. The behavior of the obtained dependencies is similar to the behavior of the square root function. The dependence shown in Fig. 11.22, demonstrates the effect of the outer diameter of the disk on the maximum output voltage and power. It

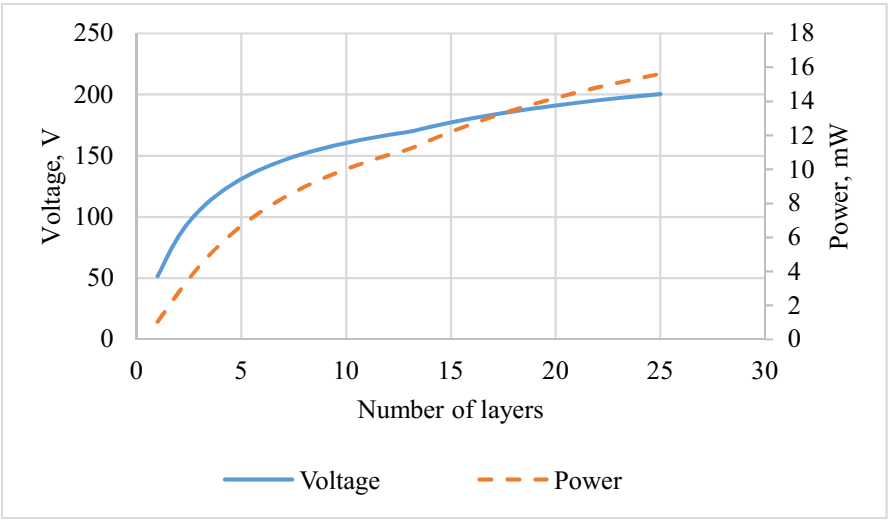


**Fig. 11.21**: Dependence of output voltage and output power of stacked PEG on the number of layers

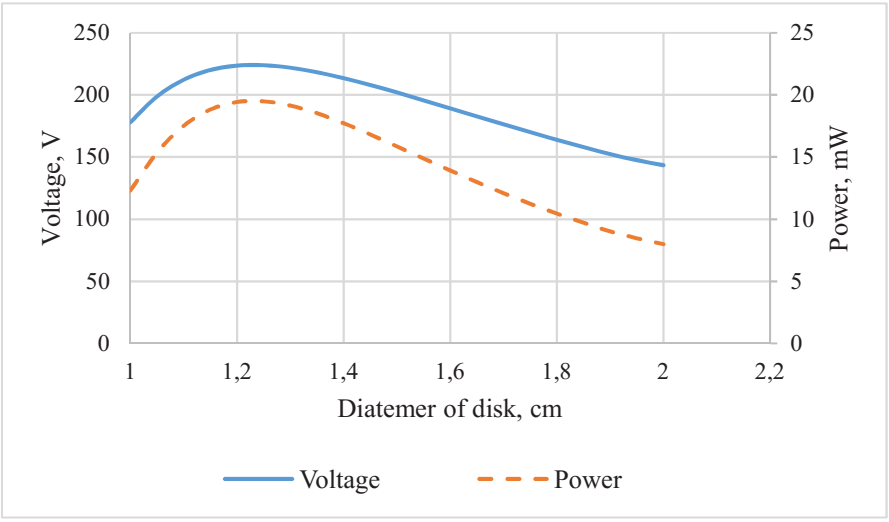


**Fig. 11.22**: Dependence of the output voltage and output power of the stacked PEG on the diameter of the piezoelectric cell

Table 11.2: PEG Parameters

| | Core | Piezoelement |
|---|---|---|
| Geometrical dimensions($D \times d \times h$) | 6 mm | 18×8×1 mm$^3$ |
| Density ($\rho$) | 7800 kg/m$^3$ | 7500 kg/m$^3$ |
| The Young's modulus and Poisson's ratio ($E, \nu$) | 210 GPa and 0.3 | — |
| Elastic compliance $\left(s_{33}^E\right)$ | — | 17×10$^{-12}$ Pa |
| Relative permittivity $\left(\varepsilon_{33}^S/\varepsilon_0\right)$ | — | 1500 |
| Piezoelectric module ($d_{33}$) | — | -307 pC/N |

follows from the figure that with an increase in the external diameter of the disk, the output voltage and power increase to a certain value, after which the recession occurs. From Fig. 11.23, which shows the dependence of the maximum output voltages and power on the height of each layer, it follows that as the height of the layers increases, the output voltages and power increase. This dependence is close to linear.

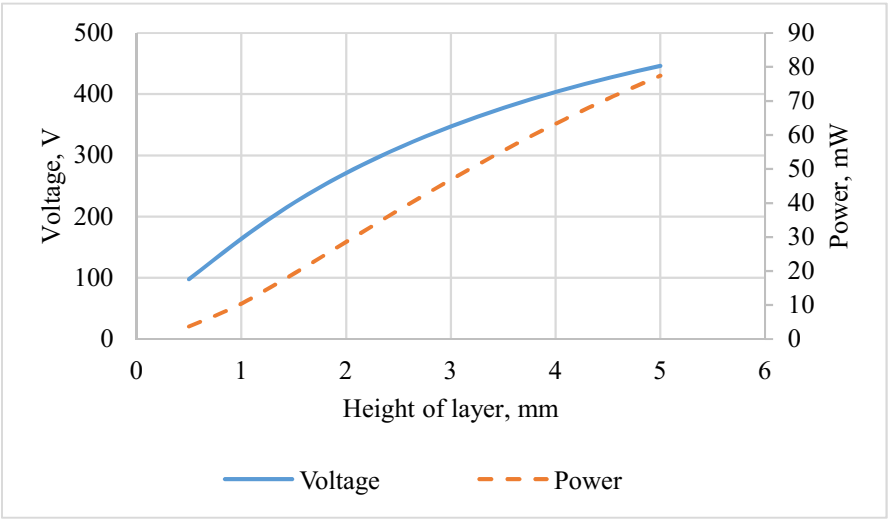


**Fig. 11.23**: Dependence of output voltage and output power of stacked PEG on the height of each layer

In addition, the influence of the number of layers on the output characteristics of PEG was investigated at a fixed total height of the entire piezostack. The results are shown in Fig. 11.24. It turned out that there is a number of layers, in which the output characteristics will be maximum.

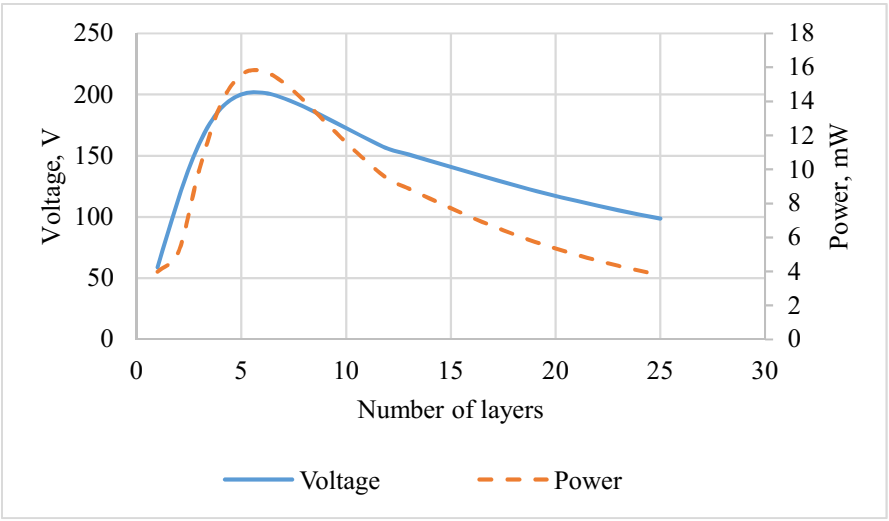


**Fig. 11.24**: Dependence of the output voltage and output power of the stacked PEG on the number of layers, provided that the height of the entire packet remains unchanged

#### 11.2.3.2 Comparison With Finite Element

Let us compare the derived model for stack PEG with finite-element calculations. In Solovyev et al (2016), a finite element simulation of the stack PEG impulse loading experiment was carried out. In the ANSYS package, the generator model was constructed. The model is presented in Fig. 11.25. In the course of the experiment, a pulse excitation aplied to the PEG was recorded, which was shown earlier in Fig. 11.20. This impulse was used in ANSYS as an excitation force. Calculation of the output electric potential was made with three values of electrical resistance: 374 kOhm, 2.6 MOhm, 22.7 MOhm. A comparison of the results obtained with finite element modeling and the analytical model is shown in Fig. 11.26. From Fig. 11.26 it follows that the model obtained coincides, with a sufficient degree of accuracy, with the finite-element calculation. The average error did not exceed 5%.

## 11.3 Summary

In this work, applied numerical theories were constructed, allowing preliminary estimations of the output characteristics of the PEG of various configurations. The developed theories are based on the Hamiltonian principle, extended to the theory of electroelasticity. The solution was carried out using the Kantorovich method. In the first part of the work, within the framework of the Euler-Bernoulli hypotheses, a

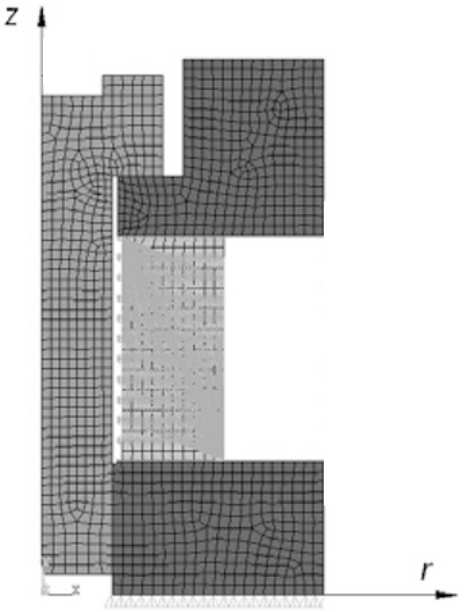


**Fig. 11.25** Axisymmetric finite element model of PEG

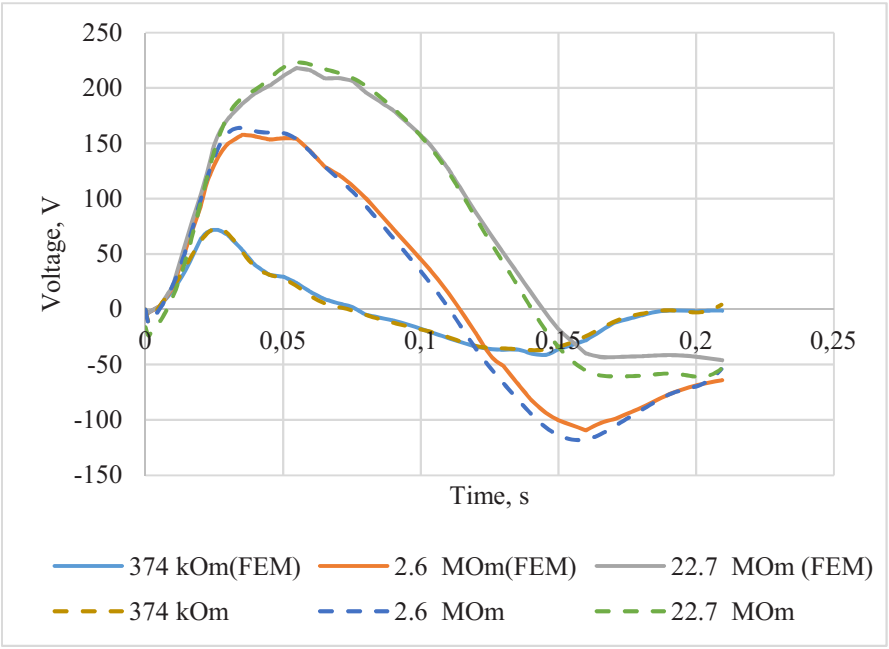


**Fig. 11.26**: The time dependence of the electrical potential for various electrical resistances: dashed line — model, continuous line — finite element simulation

model of a cantilever PEG was created. The main model's peculiarity is the consideration of structural features. In the second part, a model was developed for multilayer stacked PEG, where the energy generation process was considered as forced oscillations of an electroelastic rod. The adequacy of the obtained theories in both cases was verified by comparison with finite-element modelling. The characteristics of PEGs (resonant frequencies, output voltage and power) are calculated depending on geometric parameters such as the dimensions, location of piezoelements, the number of piezolayers, etc. The results are presented in the form of graphs of possible options for optimal parameters of PEG.

**Acknowledgements** This work has been supported by the Government Contract (project part) 9.1001.2017/PCh, by the Russian Foundation for the Basic Research Grant 16-58-52013 MNT-a and by Russian State Mission 007-01114-16 PR (project 0256-2015-0074).

## References

Adhikari S, Friswell MI, Inman DJ (2009) Piezoelectric energy harvesting from broadband random vibrations. Smart Materials and Structures 18(11):115,005

Baker J, Roundy S, Wright P (2005) Alternative geometries for increasing power density in vibration energy scavenging for wireless sensor networks. In: 3rd International Energy Conversion Engineering Conference, American Institute of Aeronautics and Astronautics

Cavallier B, Berthelot P, Nouira H, Foltete E, Hirsinger L, Ballandras S (2005) Energy harvesting using vibrating structures excited by shock. In: IEEE Ultrasonics Symposium, IEEE, vol 2, pp 943–945

Chebanenko VA, Akopyan VA, Parinov IA (2015) Piezoelectric generators and energy harvesters: Modern state of the art. In: Parinov IA (ed) Piezoelectrics and Nanomaterials: Fundamentals, Developments and Applications, Nova Science Publishers, New York, pp 243–277

Deng Q, Kammoun M, Erturk A, Sharma P (2014) Nanoscale flexoelectric energy harvesting. International Journal of Solids and Structures 51(18):3218–3225

Dutoit NE, Wardle BL (2007) Experimental verification of models for microfabricated piezoelectric vibration energy harvesters. AIAA journal 45(5):1126–1137

Dutoit NE, Wardle BL, Kim SG (2005) Design considerations for MEMS-scale piezoelectric mechanical vibration energy harvesters. Integrated Ferroelectrics 71(1):121–160

Elvin N, Erturk A (2013) Advances in Energy Harvesting Methods. Springer, Heidelberg

Erturk A, Inman DJ (2008) On mechanical modeling of cantilevered piezoelectric vibration energy harvesters. Journal of Intelligent Material Systems and Structures 19(11):1311–1325

Erturk A, Inman DJ (2011) Piezoelectric Energy Harvesting. John Wiley and Sons, Ltd., New York

Feenstra J, Granstrom J, Sodano H (2008) Energy harvesting through a backpack employing a mechanically amplified piezoelectric stack. Mechanical Systems and Signal Processing 22(3):721–734

Goldfarb M, Jones LD (1999) On the efficiency of electric power generation with piezoelectric ceramic. Trans ASME J Of Dyn Syst Measurement and Control 121:566–571

Han B, Vassilaras S, Papadias CB, Soman R, Kyriakides MA, Onoufriou T, Nielsen RH, Prasad R (2013) Harvesting energy from vibrations of the underlying structure. Journal of Vibration and Control 19(15):2255–2269

Kerr AD, Alexander H (1968) An application of the extended kantorovich method to the stress analysis of a clamped rectangular plate. Acta Mechanica 6(2-3):180–196

Liao Y, Sodano HA (2009) Structural effects and energy conversion efficiency of power harvesting. Journal of Intelligent Material Systems and Structures 20(5):505–514

Liu Y, Tian G, Wang Y, Lin J, Zhang Q, Hofmann HF (2009) Active piezoelectric energy harvesting: General principle and experimental demonstration. Journal of Intelligent Material Systems and Structures 20(5):575–585

Nechibvute A, Chawanda A, Luhanga P (2012) Finite element modeling of a piezoelectric composite beam and comparative performance study of piezoelectric materials for voltage generation. ISRN Mater Science ID 921361:11 pages

Roundy S, Wright PK (2004) A piezoelectric vibration based generator for wireless electronics. Smart Materials and Structures 13(5):1131

Shevtsov S, Akopyan V, Rozhkov E, Chebanenko V, Yang CC, Jenny Lee CY, Kuo CX (2016) Optimization of the electric power harvesting system based on the piezoelectric stack transducer. In: Parinov IA, Chang SH, Topolov VY (eds) Advanced Materials: Manufacturing, Physics, Mechanics and Applications, Springer International Publishing, Cham, pp 639–650

Soloviev AN, Vatulyan AO (2011) Non-classical biem in electroelasticity and inverse coefficient problem. In: Parinov IA (ed) Piezoceramic Materials and Devices, Nova Science Publishers, New York, pp 1–51

Soloviev AN, Parinov IA, Duong LV, Yang CC, Chang SH, Lee JCY (2013) Analysis of finite element models for piezoelectric devices of energy harvestingm. In: Parinov IA, Chang SH (eds) Physics and Mechanics of New Materials and their Applications, Nova Science Publishers, New York, pp 335–352

Soloviev AN, Chebanenko VA, Zakharov YN, Rozhkov EV, Parinov IA, Gupta VK (2017) Study of the output characteristics of ferroelectric ceramic beam made from non-polarized ceramics pzt-19: Experiment and modeling. In: Parinov IA, Chang SH, Jani MA (eds) Advanced Materials: Techniques, Physics, Mechanics and Applications, Springer International Publishing, Cham, pp 485–499

Solovyev AN, Duong LV (2016) Optimization for the harvesting structure of the piezoelectric bimorph energy harvesters circular plate by reduced order finite element analysis. International Journal of Applied Mechanics 8(3):1650,029

Solovyev AN, Duong LV, Akopyan VA, Rozhkov EV, Chebanenko VA (2016) Numerical simulation of the experiment on pulsed excitation of stack type piezoelectric generator. Vestnik DSTU 1(84):19–26

Vatulyan AO, Soloviev AN (2009) Direct and inverse problems for homogeneous and inhomogeneous elastic and electroelastic bodies (in Russ.). SFEDU Publishers, Rostov-on-Don

Wang J, Shi Z, Han Z (2013) Analytical solution of piezoelectric composite stack transducers. Journal of Intelligent Material Systems and Structures 24(13):1626–1636

Yu S, He S, Li W (2010) Theoretical and experimental studies of beam bimorph piezoelectric power harvesters. J of Mechanics of Mater and Structures 5(3):427–445

Zhao S, Erturk A (2014) Deterministic and band-limited stochastic energy harvesting from uniaxial excitation of a multilayer piezoelectric stack. Sensors and Actuators A: Physical 214:58–65